

# When Good Equations Get Bad Scores: Improving Symbolic Regression Through Better Parameter Optimization

Boxiao Wang<sup>1</sup>, Kai Li<sup>1\*</sup>, Zhiwei Chen<sup>1</sup>, Yang Huang<sup>1</sup>,  
Runxiang Wang<sup>1</sup>, Ziwen Zhang<sup>1</sup>, Yifan Zhang<sup>1</sup>, Jian Cheng<sup>1</sup>

<sup>1</sup>Institute of Automation, Chinese Academy of Sciences

## Abstract

Symbolic Regression (SR) plays a central role in scientific knowledge discovery by distilling mathematical equations from observational data. Most existing SR methods function within a bi-level optimization framework: an outer loop that searches for the discrete equation structure, and an inner loop that optimizes the continuous parameters of that structure. Crucially, parameter-fitting quality directly determines a structure’s score and thus the outer-loop search. However, nonlinear operators make the inner loop highly non-convex, and budget-driven reliance on fast local solvers (e.g., BFGS) often yields poor local minima and underestimated scores for correct structures. This “Good Structure, Bad Score” phenomenon becomes a key bottleneck, degrading efficiency and misguiding the search away from the true equation. To resolve this, we propose **SAGE-Fit** (Structure-Aware and Semantics-Guided Evaluator for Symbolic Regression), an SR-native fitting framework that exploits the *dual native priors* of symbolic expressions. By capitalizing on the structural and semantic priors unique to SR, we design tailored modules for each property, thereby effectively mitigating this optimization bottleneck. Extensive experiments demonstrate that our approach, as a plug-and-play module, significantly enhances evaluation fidelity and universally improves the performance of various SR systems.

## 1 Introduction

Symbolic Regression (SR) differs from traditional regression by simultaneously searching for optimal equation structures and the associated parameters, with the goal of discovering interpretable physical laws from data (Schmidt and Lipson 2009; Billard and Diday 2002). While methodologies have evolved from genetic programming (Koza 1994; Schmidt and Lipson 2009; Virgolin, Alderliesten, and Bosman 2019) to reinforcement learning (Petersen et al. 2021; Landajuela et al. 2022; Hayes et al. 2025; Li et al. 2024) and large language models (Shojaee et al. 2025; Merler et al. 2024; Hua et al. 2025; Grayeli et al. 2024), the underlying paradigm remains a **bi-level optimization framework**. This framework consists of an outer loop that proposes discrete equation skeletons (e.g., expression trees or token sequences) and an inner loop that optimizes the continuous constants (parameters) within these structures. Ideally, this decomposition allows the outer loop to focus on

structural exploration while the inner loop handles numerical fitting. However, we identify a critical asymmetry in current SR research: while the outer loop has benefited from sophisticated architectural innovations, the inner loop largely relies on generic local optimizers such as BFGS or Nelder-Mead (Udrescu and Tegmark 2020; dos Reis, Caminha, and Penna 2024). This reliance assumes that these fast solvers can reliably assess the quality of a structure. In reality, nested nonlinear operators (e.g., exponentials and trigonometric functions) create a highly non-convex loss landscape with numerous local minima—a “needle-in-a-basin” topology that generic optimizers struggle to navigate. Consequently, structurally correct equations often receive poor fitness scores because the local optimizer fails to locate the global parameters, a phenomenon we term “**Good Structure, Bad Score.**” The repercussions of this inner-loop failure are twofold. First, it degrades *evaluation fidelity*: the search algorithm is misled to discard promising candidates, which prevents convergence to the true physical law. Second, it wastes computational resources on repeated, ineffective optimization attempts. As demonstrated in our experiments, even when the outer loop successfully identifies the exact ground-truth skeleton, standard optimizers frequently fail to fit the parameters, rendering the discovery process futile. Thus, the bottleneck of modern SR has shifted from the generation of valid structures to the accurate evaluation of these structures. To understand when and why this happens, we conduct a landscape-level case analysis that characterizes optimization failures in SR from two complementary viewpoints: correct-structure landscapes and landscapes of partially correct structures. Instead of relying on black-box continuous solvers that ignore equation structures, we argue that a highly faithful evaluator must inherently respect the distinct nature of symbolic expressions. To this end, we propose **SAGE-Fit** (Structure-Aware and Semantics-Guided Evaluator for Symbolic Regression), a unified parameter fitting framework that explicitly exploits the *dual native priors* of symbolic equations. Specifically, to target the structural prior, we leverage the hierarchical parameter distribution within the expression tree to design a *Tree-Directed Variable Projection* that deterministically decouples conditionally linear parameters; concurrently, by utilizing the explicitly known analytic equation structure upon the reduced non-linear manifold, we formulate an SR-specialized *Pro-*

\*Corresponding author.

jected *Gauss–Newton* method to achieve highly efficient local convergence. To target the semantic prior, we address the critical risk of basin collapse inherent to random parameter-space initialization by introducing *Semantics-Guided Initialization*. By evaluating the actual input-output behavioral mappings of candidates rather than relying on deceptive distances in the parameter space, we design a *Function-Space Farthest-Point Sampling* (FS-FPS) mechanism to guarantee that the starting points are maximally diverse in their true semantic behavior. Finally, we integrate these unified modules as a plug-and-play evaluator into representative SR frameworks spanning genetic programming, reinforcement learning, and LLM-based candidate generation. Across these diverse settings, upgrading the inner-loop optimizer consistently improves both symbolic accuracy and numerical fidelity, thereby demonstrating that enhancing inner-loop optimization alone can substantially strengthen mainstream SR systems.

## 2 Related Work

With the increasing adoption of two-part SR paradigms, the structure discovery module determines the operators and compositional form of the expression, while parameter fitting module refines the numerical constants via continuous optimization algorithms under the fixed structure. This decomposed strategy substantially reduces the complexity of the overall search space, decouples structure discovery from parameter estimation and improves the reliability and stability of candidate structure evaluation. Since this work focuses on the bi-level formulation, we review prior studies from two complementary perspectives: (i) outer-loop structure search, and (ii) inner-loop parameter optimization.

### 2.1 Structure Search

Early SR methods primarily relied on deterministic modeling and sparse regression, such as FFX (McConaghy 2011; Vaddireddy and San 2019; Kammerer, Kronberger, and Kommenda 2022) and SINDy (Brunton, Proctor, and Kutz 2016a,b; Udrescu and Tegmark 2020). These methods exhibit high efficiency and stability when the hypothesis space is constrained to a predefined library of basis functions; however, their expressive power is largely limited by the design of the function library. To expand the searchable function space, genetic programming (GP)-based SR methods have been extensively studied (Koza 1994; Schmidt and Lipsen 2009; Virgolin, Alderliesten, and Bosman 2019). These methods typically represent expressions as trees and perform global search over the symbolic composition space via evolutionary operators such as mutation and crossover. Building upon this paradigm, methods such as PySR (Cranmer 2023) further adopt multi-objective formulations for candidate selection, leading to improved search efficiency and expression quality. With the advancement of neural network methodologies, SR has increasingly been combined with neuro-symbolic and search-driven approaches. For instance, Equation Learner (EQL) replaces standard neural network activation functions with interpretable mathematical operators (Martius and Lampert 2016; Sahoo, Lampert, and Mar-

tius 2018; Dong et al. 2024), enabling the learning of symbolically meaningful functional connections. Other methods, including DSR (Petersen et al. 2021), DSO (Landajuela et al. 2022; Hayes et al. 2025), and DSN (Li et al. 2024), formulate SR as a sequential decision-making problem and employ reinforcement learning to explore the expression space. In addition, several studies integrate Monte Carlo Tree Search (MCTS) with deep generative models to enhance global exploration and the stability of symbolic expression search (Kamienny et al. 2023; Huang et al. 2025). More recently, SR has witnessed growing interest in large language model (LLM)-driven approaches (Shojaee et al. 2025; Merler et al. 2024; Hua et al. 2025; Grayeli et al. 2024). Benefiting from strong capabilities in code generation and symbolic reasoning, these models are used to propose symbolic expressions or programmatic equation templates. Furthermore, retrieval-augmented methods such as RAG-SR incorporate external or historical expressions through retrieval-augmented generation mechanisms, thereby improving the stability and quality of generated symbolic models (Zhang et al. 2025; Guo et al. 2025).

### 2.2 Parameter Optimization

Early GP-based SR often performed constant fitting using local or stochastic search methods such as hill climbing (Koza 1994) and simulated annealing (Stinstra, Rennen, and Teeuwen 2008; Kantor, Von Zuben, and de Franca 2021). To improve robustness under highly non-convex objectives, subsequent work introduced population-based, gradient-free optimizers, including genetic algorithms (Alonso, Montana, and Borges 2009), particle swarm optimization (Loebl and Rozinajová 2018; Sheta et al. 2023), and differential evolution (Cerny, Nelson, and Zhou 2008). These derivative-free approaches are generally less sensitive to poor local geometry, but can be sample-inefficient and may converge slowly or yield suboptimal numerical accuracy. With the increasing prevalence of bi-level SR pipelines, the inner-loop fitting problem is typically solved by continuous optimizers specialized for regression-style objectives. Many systems rely on fast local optimizers such as quasi-Newton methods (e.g., BFGS) or simplex-based methods (e.g., Nelder–Mead) for rapid error reduction (Cranmer 2023; Petersen et al. 2021). When the objective can be cast as (or approximated by) nonlinear least squares, least-squares solvers such as Levenberg–Marquardt are also commonly used for refinement (Burlacu, Kronberger, and Kommenda 2020). In neural-network-based SR, parameter adjustment is typically carried out during training via gradient-based optimization, while additional local refinement may be applied to obtain precise constants for the final symbolic form (Martius and Lampert 2016; Sahoo, Lampert, and Martius 2018; Li et al. 2024). These choices are reflected across representative SR systems: PySR fits constants for candidate trees using local optimizers such as BFGS or Nelder–Mead (Cranmer 2023); Operon performs post-hoc refinement using Levenberg–Marquardt least-squares optimization (Burlacu, Kronberger, and Kommenda 2020); DSR refits constants using gradient-based optimizers (e.g., BFGS) and uses the optimized error as the

learning signal for structure search (Petersen et al. 2021); and LLM-SR iteratively updates parameters via automatic differentiation coupled with optimizers such as Adam or BFGS (Shojaee et al. 2025).

### 3 Preliminary

#### 3.1 Symbolic Regression Task

In SR (Makke and Chawla 2024), the learning task typically starts with a dataset consisting of input–output pairs:

$$D = \{(\mathbf{x}_i, y_i)\}_{i=1}^n, \quad \mathbf{x}_i \in \mathbb{R}^d, y_i \in \mathbb{R}, \quad (1)$$

where  $\mathbf{x}_i$  denotes a  $d$ -dimensional input vector and  $y_i$  is the corresponding scalar output. The goal is to discover an explicit analytic equation  $f(\cdot)$  such that the predicted outputs  $\hat{y}_i = f(\mathbf{x}_i)$  accurately approximate the ground-truth targets  $y_i$ , while maintaining robust generalization to unseen inputs.

#### 3.2 Equation Structures and Parameter Fitting

**Equation structures.** In many SR methods, a candidate equation is commonly viewed as being determined jointly by a *discrete symbolic structure* and *continuous numerical parameters*. The former specifies the operator symbols, variable symbols, and their combinatorial arrangement (e.g., an expression tree or a computational graph), while the latter comprises numerical quantities that must be estimated from data (e.g., constants, coefficients, frequencies, and phases). Motivated by this widely adopted framework, we define an *equation structure* as follows: all numerically unspecified components in an expression are abstracted as *parameter placeholder*, while the discrete symbolic structure is kept unchanged. For example,  $\sin(2x)$  and  $\sin(3.3x + \pi)$  can be regarded as instances of the same structure  $\sin(ax + b)$ , where  $a$  and  $b$  are parameters to be fitted. Formally, a structure induces a parametric function family

$$f(\cdot; \theta) : \mathcal{X} \rightarrow \mathbb{R}, \quad \theta \in \Theta_f \subset \mathbb{R}^{d_f}, \quad (2)$$

where  $\mathcal{X} \subseteq \mathbb{R}^d$  denotes the input space,  $\Theta_f$  is the parameter space associated with the structure  $f$ , and  $d_f$  is the parameter dimension (i.e., the number of parameter slots).

**Parameter fitting.** Given a fixed structure  $f$ , parameter fitting aims to estimate optimal parameters from the dataset  $D = \{(\mathbf{x}_i, y_i)\}_{i=1}^n$ . We typically define the empirical loss in terms of the mean squared error (MSE):

$$L_f(\theta; D) = \frac{1}{n} \sum_{i=1}^n (y_i - f(\mathbf{x}_i; \theta))^2. \quad (3)$$

The parameter fitting problem for the structure can then be formulated as

$$\theta_f^*(D) \in \arg \min_{\theta \in \Theta_f} L_f(\theta; D). \quad (4)$$

It is worth noting that, unlike linear models of the form “basis functions + coefficients”, SR often involves parameters that appear inside nonlinear operators (e.g.,  $\sin(\theta x)$ ,  $x^\theta$ ,  $\exp(\theta x)$ ), which may render  $L_f(\theta; D)$  a non-convex objective.

## 4 Anatomy of Fitting Failures

In SR, fitting failures are predominantly tied to the nonconvexity induced by nonlinear operators and nonlinear parameterization. When parameters enter the model linearly, coefficients can be recovered reliably via (regularized) least squares, and the fitting outcome is largely insensitive to initialization. In contrast, nonlinear parameterization makes the objective highly nonconvex and often ill-conditioned, so local solvers become initialization-sensitive and can return severely underestimated scores even for correct structures.

### 4.1 Correct-structure landscapes: SR Scoring Needle-Basin on a Rugged Landscape

In this subsection, we study the optimization landscape of structures that are structurally identical to the ground-truth equations. Unlike simple linear models, equations with nested nonlinear terms—commonly used in physics to describe oscillatory dynamics or exponential decay—often induce a highly ill-conditioned geometry (Ioannou, Liò, and Cicuta 2026; Schmidt and Lipson 2009). We refer to the characteristic geometry arising from the complex coupling of nonlinear parameters as a *Needle-Basin* (Gill and Murray 1978).

**The “Needle-in-a-Basin” Topology.** From the perspective of SR scoring, these needle-basins are embedded in a highly rugged loss surface populated with poor stationary points and flat plateaus, as shown in Figure 1. Consequently, single-start local fitters (e.g., BFGS-style methods) are prone to converging to high-error stationary points or stalling on plateaus under conventional initializations (Kommenda et al. 2020). This premature termination triggers stopping criteria early, assigning an unjustifiably poor score to an otherwise correct structure (i.e., an optimizer-induced false negative).

**Non-convexity and Multimodality.** The landscape of nonlinear SR structures is inherently multimodal. As illustrated in Figure 1, the parameter space is partitioned into multiple disconnected basins of attraction (Sergeyev, Kvasov, and Mukhametzhanov 2016; Riley, Webb, and Baker 2025). This multimodality often stems from the periodicity of trigonometric operators or the symmetry of exponential terms, creating numerous suboptimal local attractors that compete with the global solution. Standard gradient-based methods lack the mechanism to escape these suboptimal basins once initialized within them.

**Stalling and Premature Termination.** Local fitters commonly used in SR typically rely on gradient-norm–based stopping rules (e.g.,  $\|\nabla L\| < \epsilon$ ). In a rugged needle-basin landscape, once the optimizer traverses into a suboptimal attractor region or a flat plateau, the local gradient magnitudes can diminish rapidly. This satisfies the stopping criterion even though the resulting fitting error remains orders of magnitude higher than the best attainable level for that structure. This phenomenon distorts the fitness score fed back to the outer-loop search (dos Reis, Caminha, and Penna 2024; Kommenda et al. 2020), misguiding the evolutionary process.

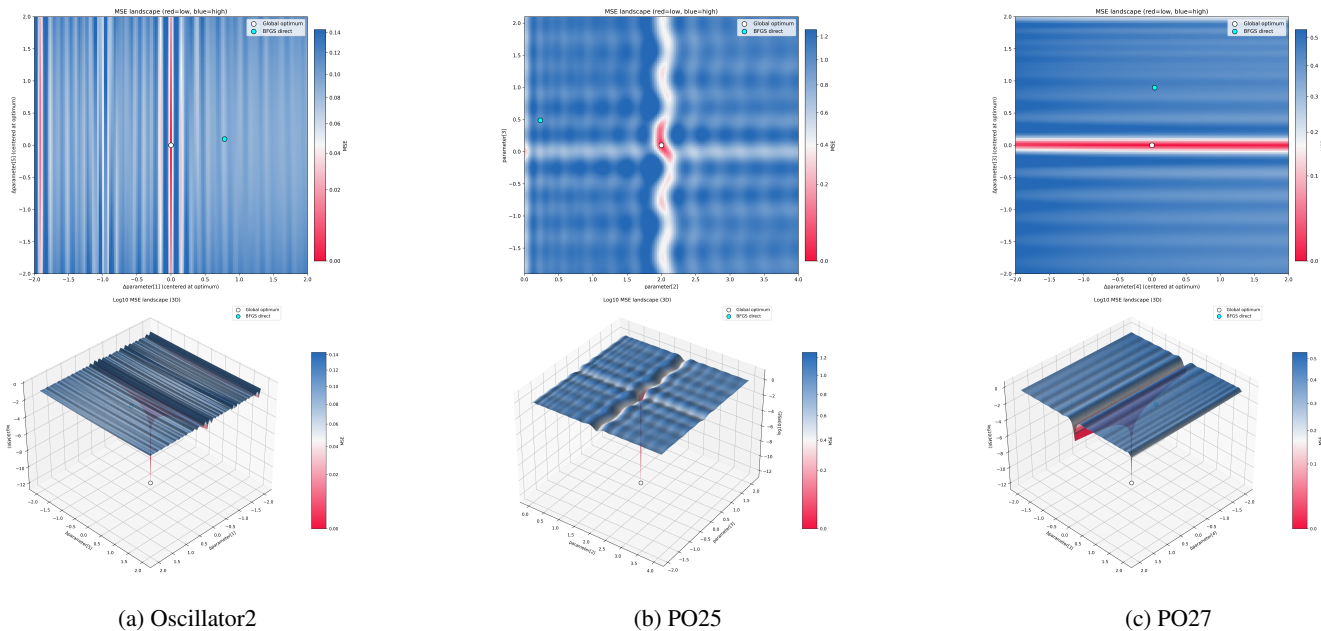


Figure 1: “Needle-in-a-basin” phenomenon in SR. We select three representative cases from llmsrbench. For each task, we visualize the MSE loss landscape with a 2D slice (top) and a 3D view (bottom).

## 4.2 Landscapes of Partially Correct Structures: Diverse and Unstable Fitting Behaviors

In this subsection, we investigate the parameter optimization landscapes associated with partially correct structures. Here, a candidate structure is defined as “partially correct” if it deviates from the ground-truth equation solely through localized structural modifications (e.g., the omission of a term or the substitution of a local operator). In contrast to the correct structures discussed in Section 4.1—which typically exhibit a consistent needle-basin geometry—we observe **diverse and unstable fitting behaviors** for partially correct structures (see Fig. 2). Specifically, the loss landscapes and resulting optimization trajectories vary markedly, characterized by three recurring phenomena (Kronberger and de Franca 2025). First, low-error regions often manifest as **needle-basin pockets** or trenches; in certain cross-sections, multiple isolated low-error pockets are observable. Second, we frequently observe **multiple competitive basins**, where several disconnected basins with comparable minimum errors coexist, implying that the solution yielding a low error is not unique. Finally, the landscape may feature **wide valleys with high barriers**: although the optimal valley can be relatively broad, it is often separated from sub-optimal basins by significant energy barriers or narrow passages.

## 5 Method

Section 4 demonstrates that the optimization landscape of the SR inner loop is characterized by two primary failure modes: severe ill-conditioning (needle-in-a-basin landscapes) for correct structures, and competing low-error basins for partially correct structures. These issues arise be-

cause the structure of the symbolic expression is typically treated as a black box. A generic continuous optimizer observes only the parameter vector  $\theta \in \mathbb{R}^d$  and the loss function  $L(\theta)$ , thereby ignoring two strong priors inherent to the construction of an SR candidate. The first prior is *algebraic*: the expression tree determines which parameters enter the residual through affine transformations and which are genuinely non-linear. The second prior is *semantic*: the outer loop ultimately evaluates the function induced on the data, rather than the specific parameter coordinates that generate it. We utilize these two priors as the foundational design principles for the inner-loop optimizer, integrating them into a unified evaluator named **SAGE-Fit** (Structure-Aware and Semantics-Guided Evaluator for Symbolic Regression).

### 5.1 Rethinking Parameter Optimization in SR

Given a candidate structure  $T$  with a parameter vector  $\theta \in \mathbb{R}^d$  and  $n$  training points, the ideal inner-loop score is the optimal mean squared error

$$\mathcal{S}(T) = \min_{\theta \in \Theta_T} \frac{1}{n} \|\mathbf{y} - f_T(\mathbf{X}; \theta)\|_2^2. \quad (5)$$

However, the outer loop typically receives a budget-limited estimate  $\widehat{\mathcal{S}}(T) = \frac{1}{n} \|\mathbf{y} - f_T(\mathbf{X}; \hat{\theta})\|_2^2$ , where  $\hat{\theta}$  represents the parameter configuration returned by the inner-loop optimizer under a fixed computational budget. Throughout this section, every residual norm  $\|\cdot\|_2^2$  utilized as a loss, score, or trigger quantity is normalized by  $n$ ; thus, all loss values correspond to the mean squared error. The non-negative gap

$$\Delta(T) = \widehat{\mathcal{S}}(T) - \mathcal{S}(T) \geq 0 \quad (6)$$

is defined as the *score distortion*. When  $\Delta(T)$  is exceptionally large for a structurally promising candidate  $T$ , the outer

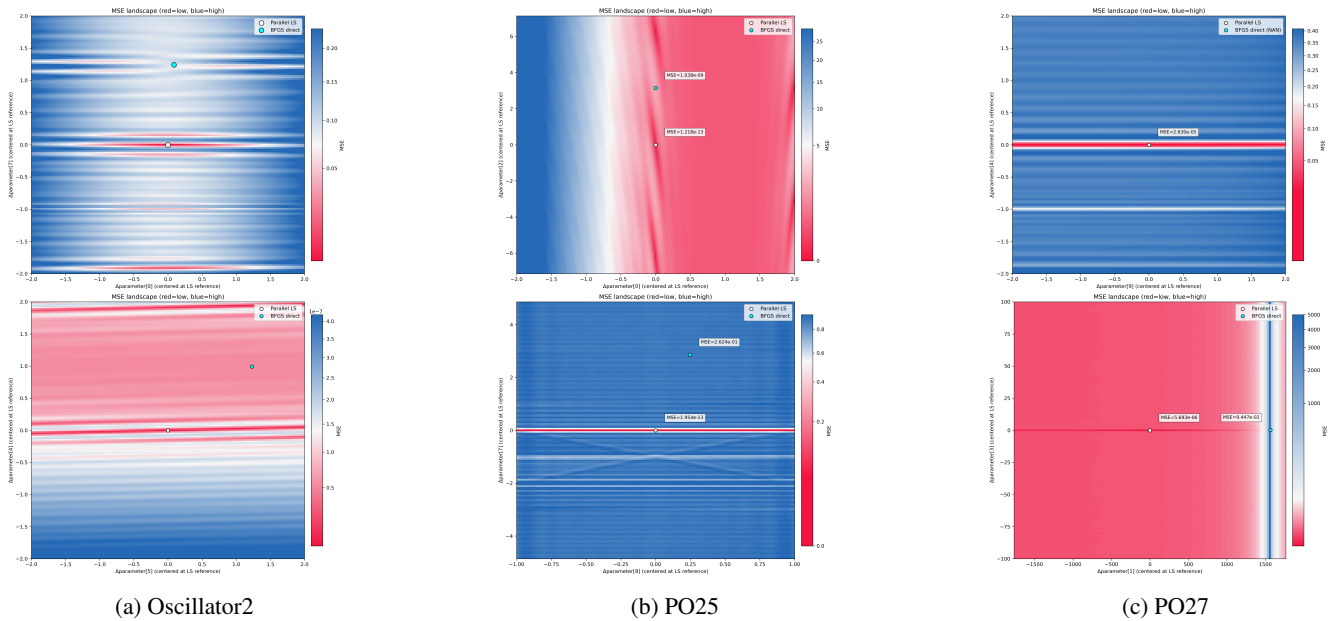


Figure 2: Non-convexity and multimodality in nonlinear SR: disconnected basins and local-optimum traps.

loop incorrectly discards the structure. This phenomenon constitutes an optimizer-induced false negative, which is quantified empirically in Section 4. Consequently, reducing  $\Delta(T)$  *uniformly across all candidates*, rather than merely improving the accuracy of any single fitting process, serves as the central design objective for an evaluator tailored to symbolic regression. A generic continuous optimizer minimizes the objective in (6) relying strictly on standard descent methodologies. Instead, two fundamental properties of a symbolic candidate, which are universally available yet frequently ignored, can be systematically exploited.

**Algebraic structural prior.** The expression  $T$  is represented as an abstract syntax tree (AST). Traversing this tree reveals which parameters enter the residual *affinely* (i.e., conditionally linear parameters) and which are genuinely non-linear. This exact decomposition is directly derived from the algebraic structure of the tree and effectively reduces the dimensionality of the non-linear search space.

**Functional semantic prior.** The critical component for evaluation is the function mapping  $\mathbf{x} \mapsto f_T(\mathbf{x}; \theta)$  over the dataset, rather than the specific coordinates of the parameter vector  $\theta$ . Distances in the parameter space  $\theta$  are frequently misleading; for instance,  $a \sin(bx + c) = (-a) \sin(bx + c + \pi)$ . Therefore, a faithful measure of diversity must be defined based on the observed functional behavior rather than on parameter coordinates. In the remainder of this section, we operationalize each prior into a concrete mechanism (Sections 5.2, 5.3, and 5.4) and integrate them to formulate the adaptive SAGE-Fit evaluator (Section 5.5).

## 5.2 Module 1: Structure-Aware Dimensionality Reduction

**The Bottleneck.** Traditional optimizers treat all parameters uniformly, placing them within the same high-dimensional search space regardless of whether they enter the equation linearly or non-linearly. This uniform treatment forces the optimizer to navigate a mixed landscape where linear coefficients (e.g., amplitudes in  $a \sin(bx + c)$ ) are entangled with genuinely non-linear parameters (e.g., frequency  $b$  and phase  $c$ ). The resulting coupling significantly inflates the effective dimensionality and introduces spurious ill-conditioning.

**Deterministic Dimension Collapse via Variable Projection.** We exploit the *structural prior* inherent in symbolic expressions: by parsing the abstract syntax tree (AST) of the equation, we automatically identify which parameters are conditionally linear. These are parameters for which the equation becomes affine when all other parameters are held fixed. Concretely, we traverse the AST of candidate  $T$  and certify that the parameter  $\theta_k$  is conditionally linear if and only if

$$\frac{\partial f_T}{\partial \theta_k} \text{ is independent of } \theta_k, \quad \text{and} \quad f_T|_{\theta_k=0} \text{ contains no } \theta_k. \quad (7)$$

This condition is verified symbolically via an affine-propagation pass over the AST. Parameters satisfying both conditions form the *linear set*  $\alpha$ ; the remaining parameters constitute the *irreducible non-linear set*  $\beta$ . The candidate then admits the separable formulation

$$f_T(\mathbf{X}; \alpha, \beta) = c(\mathbf{X}; \beta) + \Phi(\mathbf{X}; \beta) \alpha, \quad (8)$$

where  $\Phi(\mathbf{X}; \beta) \in \mathbb{R}^{n \times m}$  is a basis matrix whose columns depend on the data and  $\beta$ , but remain invariant with respect to  $\alpha$ . Crucially, this decomposition allows the linear

basis to depend on the non-linear parameters. For instance, in  $a \sin(bx+c)$ , the amplitude  $a$  is absorbed into  $\alpha$  and eliminated by a linear solver, while the frequency and phase ( $b, c$ ) remain in the projected non-linear variable  $\beta$ . For any fixed  $\beta$ , the optimal  $\alpha$  is obtained in closed form via linear least squares:

$$\alpha^*(\beta) = (\Phi(\mathbf{X}; \beta)^\top \Phi(\mathbf{X}; \beta))^\dagger \Phi(\mathbf{X}; \beta)^\top (\mathbf{y} - c(\mathbf{X}; \beta)), \quad (9)$$

where  $(\cdot)^\dagger$  denotes a rank-revealing pseudo-inverse with Tikhonov regularization applied when  $\Phi^\top \Phi$  is rank-deficient. This step involves a brief, deterministic linear solution process, which is never delegated to a non-linear optimizer. The original  $d$ -dimensional problem collapses to the projected non-linear program

$$\min_{\beta \in \mathcal{B}} L_{\text{proj}}(\beta) = \frac{1}{n} \|\mathbf{y} - c(\mathbf{X}; \beta) - \Phi(\mathbf{X}; \beta) \alpha^*(\beta)\|_2^2, \quad (10)$$

whose argument resides on an irreducible non-linear manifold of dimension  $d_\beta < d$ .

**Impact.** By analytically eliminating the linear subspace, Variable Projection (VarPro) achieves a *deterministic dimension collapse*: the high-dimensional mixed search space is explicitly reduced to a lower-dimensional, purely non-linear manifold. This reduction substantially decreases optimization difficulty and removes the spurious linear-to-non-linear coupling that drives much of the needle-in-a-basin pathology described in Section 4.

### 5.3 Module 2: Semantics-Guided Initialization via Function-Space Farthest-Point Sampling

**The Bottleneck.** To escape local minima, multi-start strategies are essential. However, traditional approaches sample starting points uniformly within the *parameter space*. This strategy is fundamentally problematic for SR: the distance in the parameter space is highly deceptive. For example,  $\sin(x)$  and  $\sin(x + 2\pi)$  are semantically identical despite possessing vastly different parameter coordinates. Random sampling in the parameter space thus wastes computational budget on redundant starting points that collapse into the same basin, a phenomenon we term *basin collapse*.

**The Solution of SAGE-Fit: Diversity in Function Space, Not Parameter Space.** We introduce *Function-Space Farthest-Point Sampling* (FS-FPS), which ensures that starting points are maximally diverse in terms of their *observed behavior* on the training data, rather than their parameter coordinates. This mechanism represents the core innovation of this work. The algorithm proceeds in three steps:

1. **Oversampling:** Generate  $M = 100$  candidate parameter vectors by sampling around the warm initialization within the projected  $\beta$  space (following the VarPro dimension reduction).
2. **Function-space evaluation:** For each candidate  $\beta_m$ , compute the predicted output vector  $\mathbf{f}_m = f_T(\mathbf{X}; \alpha^*(\beta_m), \beta_m)$  on the training set. This procedure maps each parameter vector to its *semantic fingerprint*, which is the actual function it represents.

3. **Farthest-point selection:** Within the space of output vectors  $\{\mathbf{f}_m\}$ , greedily select  $K = 8$  points that are maximally separated under the normalized Euclidean distance

$$d_f(\mathbf{f}_i, \mathbf{f}_j) = \frac{\|\mathbf{f}_i - \mathbf{f}_j\|_2}{\|\mathbf{y}\|_2 + \epsilon}. \quad (11)$$

The first point is the candidate with the lowest training loss; subsequent points are chosen to maximize the minimum distance to all previously selected points.

This procedure guarantees that the  $K$  selected starting points exhibit maximal *behavioral diversity*: they produce genuinely different predictions on the training data. Consequently, they cover distinct regions of the function space and significantly reduce the risk of basin collapse.

**Why This Works.** Diversity in the parameter space does not imply diversity in the function space due to symmetries (e.g.,  $\sin(x + 2\pi k)$ ), redundancies (e.g.,  $a \sin(bx) = (-a) \sin(bx + \pi)$ ), and the non-linear warping of parameter coordinates into function outputs. By directly measuring diversity in the function space, FS-FPS ensures that each of the  $K$  starting points explores a genuinely distinct attractor basin, thereby covering the global optimum with high probability.

**Computational Cost.** The  $M$  function evaluations required for FS-FPS introduce a modest computational overhead. However, this cost is largely offset by faster convergence: because the selected starting points are of higher quality, the subsequent local optimization requires fewer iterations to reach the basin floor.

### 5.4 Module 3: SR-Specialized Local Attraction via Projected Gauss–Newton

**The Bottleneck.** Even after dimension reduction and semantic initialization, the projected non-linear manifold  $L_{\text{proj}}(\beta)$  remains highly non-convex due to trigonometric periodicity, exponential plateaus, and nested non-linearities. Standard gradient descent methods are prohibitively slow on such optimization landscapes.

**The Solution of SAGE-Fit: Curvature-Aware Descent on the Projected Manifold.** We employ a *Projected Gauss–Newton* step with Trust Region Reflective (TRF) damping, specifically tailored for the SR setting. Define the projected residual  $\tilde{r}(\beta) = \mathbf{y} - c(\mathbf{X}; \beta) - \Phi(\mathbf{X}; \beta) \alpha^*(\beta)$  and the corresponding projected Jacobian  $\tilde{J}(\beta) = \partial \tilde{r} / \partial \beta \in \mathbb{R}^{n \times d_\beta}$ . Following the Golub–Pereyra construction (Golub and Pereyra 2003), the parameter vector  $\alpha^*(\beta)$  is re-solved at every evaluation of  $\beta$  via Eq. (9). Consequently,  $\tilde{r}$  is a function of solely  $\beta$ , and  $\tilde{J}$  implicitly accounts for the dependence of  $\alpha^*$  on  $\beta$ . In this implementation,  $\tilde{J}$  is obtained through a central finite-difference pass over  $\beta$ , with  $\alpha^*$  recomputed by the same rank-guarded least squares solver at each finite-difference probe. The projected Levenberg–Marquardt step is formulated as follows:

$$\Delta \beta = - \left( \tilde{J}^\top \tilde{J} + \lambda_\beta (\text{diag}(\tilde{J}^\top \tilde{J}) + \eta I) \right)^{-1} \tilde{J}^\top \tilde{r}, \quad (12)$$

with a damping parameter  $\lambda_\beta \geq 0$  and a small numerical floor  $\eta > 0$  on the diagonal, which prevents zero values in

cases where an entry in  $\beta$  exerts no leverage on  $\tilde{r}$ . Two properties make this step particularly well suited to SR optimization landscapes. First, the Hessian-like matrix is of dimension  $d_\beta \times d_\beta$  rather than  $d \times d$ : the curvature observed by the solver represents the curvature of the irreducible manifold alone, free from the spurious coupling that conditionally linear coefficients would otherwise inject into a full Newton system. Second, the scale anisotropy across the entries of  $\beta$  (e.g.,  $\sin(\omega x)$  versus  $x^k$ ) is normalized in a coordinate-wise manner by the term  $\text{diag}(\tilde{J}^\top \tilde{J})$ .

**Impact.** Because the  $K$  starting points obtained from FS-FPS are semantically diverse and of high quality, the projected Gauss–Newton method converges rapidly to the global optimum, often requiring only a few iterations. The combination of high-quality initialization (Module 2) and rapid local convergence (Module 3) ensures that SAGE-Fit remains both reliable and computationally efficient.

## 5.5 The SAGE-Fit Evaluator

The three aforementioned modules are integrated into a unified evaluator that takes a candidate equation  $T$  as input and returns a faithful score  $\hat{S}(T)$ , along with the fitted parameters  $(\hat{\alpha}, \hat{\beta})$ . The complete procedure is summarized in Algorithm 1 in Appendix A.

**Discussion.** SAGE-Fit renders the inner loop *prior-aware* along two orthogonal axes. The *structural prior* (Module 1) exploits the algebraic structure of the AST to deterministically collapse the search space from  $d$  dimensions to  $d_\beta < d$  dimensions, thereby eliminating spurious linear-to-non-linear coupling. The *semantic prior* (Module 2) ensures that the diversity of multiple starting points is measured in the function space rather than the parameter space. This approach prevents basin collapse and guarantees that each starting point explores a genuinely distinct region of the optimization landscape. Subsequently, Module 3 provides rapid, curvature-aware local convergence originating from these high-quality seed points. Consequently, this three-module pipeline directly addresses the two failure regimes characterized in Section 4. Specifically, the needle-in-a-basin topographies driven by linear-to-non-linear coupling are eliminated by the VarPro projection (Module 1), whereas the residual multimodality on the projected manifold is mitigated through semantic diversity during initialization (Module 2), followed by rapid local attraction (Module 3). In contrast to traditional optimizers that treat all parameters and starting points uniformly, SAGE-Fit leverages the unique structure inherent in symbolic regression to achieve both high reliability and computational efficiency.

# 6 Experiment

## 6.1 Experimental Setup

**Benchmark Datasets.** To rigorously evaluate the performance of SAGE-Fit under conditions that mimic real-world scientific discovery, we utilize the LSR-Synth dataset from the LLM-SRBench suite, which comprises 128 distinct equation discovery problems. This dataset provides two critical conditions for our study. First, it mitigates the risk of

data contamination and rote memorization often observed in LLMs by constructing equations through the composition of known scientific terms with synthetic, yet plausible, novel terms. Second, the dataset features a diverse collection of high-quality equations characterized by complex parameter structures. This complexity provides a challenging testbed that closely mirrors the “needle-in-a-basin” optimization landscape, allowing us to observe how different methods perform when parameter fitting is a primary bottleneck. More details about the dataset construction and statistics are provided in Appendix B. **Baselines.** We compare SAGE-Fit against four representative SR frameworks spanning evolutionary, deep learning, and LLM-based paradigms. We include PySR, a leading evolutionary approach coupling high-performance evolutionary search with symbolic simplification to discover interpretable equations. We also evaluate uDSR, which upgrades the traditional RNN-based controller in DSR to a pre-trained Transformer and employs neural-guided decoding to generate expression trees. Furthermore, we include LaSR, a hybrid method that distills abstract symbolic concepts from prior equations to guide the interplay between LLM generation and evolutionary search. Finally, we test LLM-SR, a program-search framework that synthesizes equation skeletons as Python functions by integrating LLM scientific knowledge with data-driven multi-island evolutionary search. To isolate the contribution of the inner-loop evaluator, we test each baseline in its original form and a modified version denoted with “+” (e.g., PySR+), where the original parameter optimization module is replaced by SAGE-Fit while keeping the outer-loop search procedure unchanged. **Evaluation Metrics.** We evaluate all methods using three standard metrics: prediction accuracy, numerical fit, and symbolic correctness. To measure prediction precision, we report the Accuracy to Tolerance ( $\text{Acc}_\tau$ ) based on the relative error. For a tolerance  $\tau$ , this is defined as

$$\text{Acc}_\tau = \frac{1}{N_{\text{test}}} \sum_{i=1}^{N_{\text{test}}} \mathbf{1} \left( \left| \frac{\hat{y}_i - y_i}{y_i} \right| \leq \tau \right).$$

We additionally report the Normalized Mean Squared Error (NMSE) to assess the overall numerical accuracy, calculated as

$$\text{NMSE} = \frac{\sum_{i=1}^{N_{\text{test}}} (\hat{y}_i - y_i)^2}{\sum_{i=1}^{N_{\text{test}}} (y_i - \bar{y})^2},$$

where  $\bar{y}$  denotes the mean of the target values. Finally, to evaluate the structural quality of the discovered expressions, we adopt the Symbolic Accuracy (SA) metric. SA measures whether the discovered equation recovers the correct symbolic form, specifically checking whether the found equation is mathematically equivalent to the ground-truth equation up to fitted constants. **Implementation Details.** To ensure a fair comparison across disparate symbolic regression frameworks, we align the computational budget by enforcing a strict time limit of 1800 seconds per equation for every method. For each baseline and its corresponding “Plus” variant, we keep all outer-loop hyperparameters identical and run the paired experiments under the same random seed, the same hyperparameter configuration, and the same GPU

Models	LSR-Synth											
	Chemistry			Biology			Physics			Material Science		
	SA(%) $\uparrow$	Acc <sub>0.1</sub> (%) $\uparrow$	NMSE $\downarrow$	SA(%) $\uparrow$	Acc <sub>0.1</sub> (%) $\uparrow$	NMSE $\downarrow$	SA(%) $\uparrow$	Acc <sub>0.1</sub> (%) $\uparrow$	NMSE $\downarrow$	SA(%) $\uparrow$	Acc <sub>0.1</sub> (%) $\uparrow$	NMSE $\downarrow$
PySR	2.78	37.14	5.30e-4	13.04	19.05	3.67e-3	0.00	16.00	4.80e-3	4.00	11.76	1.90e-5
PySR+	<b>8.33</b>	<b>43.33</b>	<b>3.88e-4</b>	<b>29.17</b>	<b>45.83</b>	<b>3.51e-3</b>	<b>2.27</b>	<b>52.63</b>	<b>2.92e-3</b>	<b>16.00</b>	<b>41.67</b>	<b>1.11e-5</b>
uDSR	11.11	54.29	4.05e-7	0.00	20.83	7.76e-2	0.00	7.50	1.19e-2	0.00	13.04	1.20e-3
uDSR+	<b>13.89</b>	<b>64.89</b>	<b>1.22e-7</b>	<b>4.17</b>	<b>23.81</b>	<b>2.37e-2</b>	<b>2.27</b>	<b>12.50</b>	<b>4.82e-3</b>	0.00	<b>15.79</b>	<b>1.06e-3</b>
LaSR	2.78	25.00	1.50e-3	0.00	0.00	3.47e-1	2.27	6.82	5.95e-3	0.00	4.00	1.50e-3
LaSR+	<b>5.56</b>	<b>27.78</b>	<b>1.38e-3</b>	<b>16.67</b>	<b>8.33</b>	<b>1.02e-3</b>	<b>6.81</b>	<b>9.09</b>	<b>3.85e-3</b>	<b>4.00</b>	<b>8.00</b>	<b>6.02e-4</b>
LLM-SR	8.33	33.33	1.91e-5	16.67	41.67	4.54e-5	4.55	36.84	1.04e-4	4.00	11.36	2.31e-5
LLM-SR+	<b>11.11</b>	<b>60.61</b>	<b>1.50e-5</b>	<b>20.80</b>	41.67	<b>1.84e-5</b>	<b>11.36</b>	<b>48.00</b>	<b>9.23e-5</b>	<b>8.00</b>	<b>15.91</b>	<b>2.05e-5</b>

Table 1: Overall performance on LLM-SRBench (Qwen2.5-7B).

environment. This design isolates the intended algorithmic change to the inner-loop parameter optimization module. For the LLM-driven approaches, including LLM-SR and LaSR, we use Qwen2.5-7B as the backbone model for candidate generation and reasoning. The baseline and “Plus” variants share the same model deployment, decoding parameters, prompt templates, and search settings, ensuring that differences in search behavior arise from evaluator feedback rather than from changes in the LLM setup.

## 6.2 Main Results

**Performance Comparison.** The main results are summarized in Table 1. Before analyzing specific metrics, we emphasize a critical implementation detail designed to ensure strict fairness. Upon the termination of the search process for all baseline methods (PySR, uDSR, LaSR, LLM-SR), we applied our proposed Strategy A to refine the parameters of the final proposed equations. We observed that this post-hoc refinement consistently reduced the Mean Squared Error (MSE) across all baselines, which confirms the superior convergence capabilities of our optimizer. Crucially, the metrics reported in the “Baseline” rows of Table 1 were computed *after* this refinement. This experimental design aims to decouple the gains derived from “better final parameter tuning” from those resulting from “better structure searching.” By standardizing the final parameter fitting step, any performance gaps observed in the “+” variants are attributable solely to the capacity of the optimizer to guide the outer loop toward more promising basins of attraction during the search process. Under this rigorous evaluation protocol, the results demonstrate that equipping existing frameworks with our optimizer yields substantial improvements across all metrics. Regarding **Enhanced Structure Discovery (SA)**, the “+” variants consistently achieve higher Symbolic Accuracy. For instance, PySR+ increases SA from 2.78% to 8.33% ( $3\times$ ), while uDSR+ attains the highest SA of 13.89% on the challenging LSR-Synth dataset. These results indicate that improved parameter optimization within the inner loop effectively mitigates the “Good Structure, Bad Score” phenomenon, thereby enabling the retention and evolution of correct skeletons that might otherwise be

discarded due to suboptimal fitting. Furthermore, in terms of **Improved Numerical Fit (Acc & NMSE)**, despite the baselines undergoing the same post-hoc refinement, the “+” methods significantly outperform them in both accuracy (Acc<sub>0.1</sub>) and numerical error (NMSE). This suggests that our optimizer assists the frameworks in navigating toward fundamentally superior structural forms with better generalizability, rather than merely fitting incorrect structures. Notably, LLM-SR+ nearly doubles the accuracy (33.33%  $\rightarrow$  60.61%) in the first group, demonstrating the synergy between LLM-generated hypotheses and precise parameter validation. **Summary.** The comprehensive improvements

observed across all metrics and baseline methods—achieved under a controlled time budget (1800 seconds)—confirm that our strategy serves as an effective, “plug-and-play” enhancer. By addressing the critical bottleneck of parameter optimization, it enables existing SR frameworks to realize their full potential without necessitating modifications to the symbolic search logic itself.

## 6.3 Quantifying Evaluator Fidelity in LLM-SR

We further analyze the identical LLM-SR runs reported above to understand how the inner-loop evaluator affects the closed-loop symbolic search. LLM-SR serves as an optimal setting for this analysis: each iteration consists of a candidate generated by the LLM, followed by numerical parameter fitting; the resulting score is then fed back into the subsequent search process. Consequently, inaccurate parameter fitting can distort the feedback signal observed by the outer loop. Throughout this analysis, the LLM, prompt template, random seed, deployment environment, outer-loop code, and the budget of 1000 calls are kept strictly fixed. The only algorithmic intervention introduced is the replacement of the original BFGS-based evaluator with SAGE-Fit. Because the scores of the evaluator are utilized as feedback, the two search trajectories are expected to diverge following the initial scoring discrepancy; this divergence constitutes a core component of the measured effect.

**Task-level log-ratio improvement.** We first quantify the final performance improvement achieved by replacing the

Domain	Log-Ratio Mean	Log-Ratio Median	Avg. Lost Rate (%)	Max Lost Rate (%)
Biology	2.52	1.91	24.06	61.79
Chemistry	4.09	1.59	22.35	44.35
Physics	1.39	0.69	6.39	20.79
Material Science	5.84	5.67	47.81	65.75

Table 2: Fine-grained diagnostics on LLM-SR trajectories.

Evaluator	Lost Rate	Mean log NMSE	Median log NMSE	Time
SAGE-Fit	<b>8.0%</b>	<b>-3.794</b>	<b>-3.728</b>	0.73s
lm.trf.multi	9.5%	-3.786	-3.705	0.84s
bfgs.multi	51.5%	-2.470	-2.508	<b>0.37s</b>

Table 3: Candidate-level fitting performance on the Structure-Progress Bank. SPB contains 200 progress-associated candidate equations extracted from real search trajectories. Lower Lost Rate and lower log NMSE are better.

original evaluator with SAGE-Fit. For each task  $i$ , we define the log-scale improvement in NMSE as

$$\rho_i = \log_{10} \left( \frac{\text{NMSE}_{\text{LLM-SR},i}}{\text{NMSE}_{\text{LLM-SR+SAGE},i}} \right). \quad (13)$$

A value of  $\rho_i > 0$  indicates that SAGE-Fit achieves a lower final NMSE, whereas the magnitude of  $\rho_i$  corresponds to the reduction in error by orders of magnitude. For instance,  $\rho_i = 2$  indicates a 100-fold reduction in NMSE. We report both the mean and the median of  $\rho_i$  across all tasks. The median reflects the typical improvement at the task level, whereas the mean captures the overall shift in the improvement distribution and remains susceptible to extreme baseline failures.

**Refit-based lost rate.** Although the log-ratio improvement measures the final gains at the task level, it does not directly reveal whether the original evaluator missed promising candidates during the search process. To diagnose this effect, we compute a refit-based lost rate based on the baseline LLM-SR trajectory. Let  $\mathcal{T} = \{e_1, e_2, \dots, e_T\}$  denote the chronological sequence of candidate equations generated during a baseline LLM-SR run. We identify a subsequence of reference updates  $\mathcal{U} = \{u_1, u_2, \dots\}$ , wherein  $u_k$  represents a candidate that strictly improves the best-so-far loss under the original evaluator. For each interval following a reference update  $u_k$ , we examine the set of discarded candidates  $\mathcal{C}_k$  that failed to update the baseline incumbent solution. Subsequently, we refit both the reference  $u_k$  and each discarded candidate  $c \in \mathcal{C}_k$  utilizing SAGE-Fit, thereby obtaining the respective losses  $L_{\text{SAGE}}(u_k)$  and  $L_{\text{SAGE}}(c)$ . A discarded candidate is classified as lost if it satisfies

$$L_{\text{SAGE}}(c) < L_{\text{SAGE}}(u_k). \quad (14)$$

This condition implies that the candidate would have outperformed the incumbent solution under the high-fidelity evaluator, even though it was not recognized as an improvement

by the original evaluator. The lost rate is formally defined as

$$\text{LostRate} = \frac{\sum_k \sum_{c \in \mathcal{C}_k} \mathbb{I}[L_{\text{SAGE}}(c) < L_{\text{SAGE}}(u_k)]}{N_{\text{compared}}}, \quad (15)$$

where  $N_{\text{compared}}$  denotes the total number of discarded candidates for which both the candidate and the reference update can be successfully refitted. This metric serves as a counterfactual diagnostic of evaluator fidelity at the trajectory level, rather than a direct measurement of the quality of the final formula. Table 2 presents two complementary aspects of evaluator fidelity. First, the median of the log-ratio is positive across all domains, indicating that a typical task benefits from the replacement of the original evaluator with SAGE-Fit. This effect is most pronounced in the domain of Material Science, where the median log-ratio reaches 5.67, which corresponds to a reduction in NMSE by more than five orders of magnitude. The domains of Biology and Chemistry also exhibit substantial median improvements, achieving median log-ratios of 1.91 and 1.59, respectively. The domain of Physics exhibits a more moderate yet consistently positive median improvement of 0.69, suggesting that for highly oscillatory tasks, the remaining bottleneck may increasingly reside in the proposal of structures rather than solely in the parameter fitting process. Second, the refit-based lost rate demonstrates that the original evaluator can significantly distort decisions during the search process. A high lost rate indicates that numerous candidates discarded by the baseline trajectory emerge as highly competitive after being refitted by SAGE-Fit. This observation provides direct empirical support for the ‘‘Good Structure, Bad Score’’ hypothesis: promising expressions can be successfully generated by the outer loop, yet they fail to guide the subsequent search because their parameters are not fitted with sufficient fidelity. This effect reaches its peak in the domain of Material Science, where the average lost rate escalates to 47.81%. Overall, this analysis demonstrates that SAGE-Fit enhances LLM-SR through two interrelated mechanisms. At the level of the final output, it shifts the distribution of the task-level NMSE by multiple orders of magnitude across several domains. At the trajectory level, it mitigates the incidence of evaluator-induced false negatives by recovering structurally correct candidates that the original evaluator failed to score competitively. These results corroborate the perspective that the fidelity of the inner-loop evaluator constitutes a major bottleneck in closed-loop LLM-guided symbolic regression.

## 6.4 Structure-Progress Bank: Candidate-Level Missed Progress

The trajectory-level diagnostics in Section 6.3 reveal that inaccurate inner-loop evaluation can distort the closed-loop search process. To further isolate this effect at the candidate level, we construct a diagnostic benchmark, termed the **Structure-Progress Bank** (SPB). Unlike standard SR benchmarks that evaluate only the final output of a search algorithm, SPB focuses on candidate equations that arise within real search trajectories and are associated with observable score improvements during the search process. Specifically, we extract 200 candidate equations from 20 problems, with 10 progress-associated candidates per problem. Each selected candidate corresponds to an event in which the search trajectory exhibits an improvement in score, making the resulting bank a targeted collection of structures that the outer loop has already found potentially useful. Each candidate is represented as a callable symbolic expression with free continuous parameters. The number of parameters ranges from 2 to 11, with a median of 7. All optimizers are evaluated from the same cold-start initialization,  $\theta_0 = \mathbf{1}$ , so that SPB measures the ability of an evaluator to recover a useful fit without relying on trajectory-specific warm starts. We compare three evaluators: the traditional multi-start L-BFGS-B baseline (`bfgs_multi`), a stronger multi-start trust-region least-squares baseline (`lm_trf_multi`), and SAGE-Fit with function-space farthest-point start selection (FS-FPS). Both SAGE-Fit and `lm_trf_multi` use the same number of final local solver calls ( $K = 8$ ), while SAGE-Fit additionally performs a lightweight function-space oversampling step to select diverse starts. This setup allows us to distinguish the benefit of function-space start selection from the benefit of simply using multiple local restarts.

**Empirical reference score and SPB lost rate.** For each candidate equation  $T_i$ , we define an empirical reference score as the best NMSE achieved by any of the compared evaluators:

$$O_{\text{emp}}(T_i) = \min_{o \in \mathcal{O}} S_o(T_i),$$

$$\mathcal{O} = \{\text{bfgs\_multi}, \text{lm\_trf\_multi}, \text{SAGE-Fit}\}. \quad (16)$$

where  $S_o(T_i)$  denotes the NMSE obtained by optimizer  $o$  on candidate  $T_i$ . We emphasize that  $O_{\text{emp}}$  is not a global oracle; it is a best-achieved empirical reference among the evaluated optimizers. An optimizer is considered to miss a candidate if its fitted NMSE is substantially worse than this empirical reference:

$$\text{LostRates}_{\text{SPB}}(o; \tau) = \frac{\#\{T_i : S_o(T_i) > \tau \cdot O_{\text{emp}}(T_i)\}}{|\mathcal{B}_{\text{SPB}}|}, \quad (17)$$

where  $\tau = 3.0$  in our experiments. This metric captures candidate-level missed progress: a high lost rate indicates that an evaluator often assigns poor scores to candidates that other evaluators can fit substantially better.

Table 3 shows that SAGE-Fit substantially reduces missed-progress candidates compared with the traditional

multi-start L-BFGS-B evaluator. The lost rate decreases from 51.5% to 8.0%, representing an 84.5% relative reduction. The comparison with `lm_trf_multi` is more subtle. The two methods achieve nearly identical bulk fitting accuracy: their mean log NMSE differs by only 0.008. However, SAGE-Fit attains a slightly lower SPB lost rate, 8.0% versus 9.5%. We also observe that the difficulty of SPB increases with parameter dimension. For candidates with at most six parameters, both SAGE-Fit and `lm_trf_multi` rarely miss progress-associated candidates. For higher-dimensional candidates, the lost rate increases for both TRF-based methods, while `bfgs_multi` remains consistently fragile across almost all dimensions. This pattern suggests that parameter dimensionality alone does not fully determine evaluator failure; rather, failures arise from the interaction between dimensionality, nonlinear parameterization, and basin accessibility. Overall, SPB provides candidate-level evidence for the mechanism underlying the end-to-end gains observed above. The benchmark shows that traditional optimizers can assign poor scores to candidate equations that are fit substantially better by SAGE-Fit. Against L-BFGS-B, this effect is large and systematic. Against a stronger TRF baseline, the advantage of SAGE-Fit is concentrated in tail robustness: it reduces the probability that a progress-associated candidate is missed due to unfavorable initialization or basin collapse. These results complement the trajectory-level lost-rate analysis in Section 6.3 and further support the view that improving evaluator fidelity helps prevent promising symbolic structures from being discarded during search.

## 7 Conclusion

This work addresses a critical bottleneck in symbolic regression (SR): the ‘‘Good Structure, Bad Score’’ phenomenon. An analysis of the optimization landscape reveals that the intrinsic non-convexity and the ‘‘needle-in-a-basin’’ topology of physical equations frequently cause standard continuous optimizers to fail. Consequently, these failures underestimate the achievable scores and lead search algorithms to erroneously discard ground-truth structures. This misalignment hinders the discovery of complex scientific laws by systematically biasing the outer-loop search against highly promising candidates. To resolve this issue, we propose **SAGE-Fit**, an SR-native parameter evaluator that explicitly exploits the inherent structural and semantic priors of symbolic expressions. By integrating structure-aware dimensionality reduction with semantics-guided initialization and a specialized Projected Gauss–Newton method, SAGE-Fit overcomes the limitations of uniform parameter treatment. Integrated as a plug-and-play module into existing frameworks, this evaluator demonstrates superior performance. Extensive experiments establish that upgrading the inner-loop optimizer universally improves both symbolic accuracy and numerical fidelity without requiring alterations to the logic of the outer loop. Furthermore, evaluations utilizing the refit-based lost rate metric reveal that up to 65% of discarded candidates in certain domains could have been competitive had they been fitted with higher fidelity.

## References

- Alonso, C. L.; Montana, J. L.; and Borges, C. E. 2009. Evolution strategies for constants optimization in genetic programming. In *2009 21st IEEE International Conference on Tools with Artificial Intelligence*, 703–707. IEEE.
- Billard, L.; and Diday, E. 2002. Symbolic regression analysis. In *Classification, clustering, and data analysis: recent advances and applications*, 281–288. Springer.
- Brunton, S. L.; Proctor, J. L.; and Kutz, J. N. 2016a. Discovering governing equations from data by sparse identification of nonlinear dynamical systems. *Proceedings of the national academy of sciences*, 113(15): 3932–3937.
- Brunton, S. L.; Proctor, J. L.; and Kutz, J. N. 2016b. Sparse identification of nonlinear dynamics with control (SINDYc). *IFAC-PapersOnLine*, 49(18): 710–715.
- Burlacu, B.; Kronberger, G.; and Kommenda, M. 2020. Operon C++ an efficient genetic programming framework for symbolic regression. In *Proceedings of the 2020 genetic and evolutionary computation conference companion*, 1562–1570.
- Cerny, B. M.; Nelson, P. C.; and Zhou, C. 2008. Using differential evolution for symbolic regression and numerical constant creation. In *Proceedings of the 10th annual conference on Genetic and evolutionary computation*, 1195–1202.
- Cranmer, M. 2023. Interpretable Machine Learning for Science with PySR and SymbolicRegression.jl. arXiv:2305.01582.
- Dong, J.; Zhong, J.; Liu, W.-L.; and Zhang, J. 2024. Evolving equation learner for symbolic regression. *IEEE Transactions on Evolutionary Computation*.
- dos Reis, L.; Caminha, V.; and Penna, T. 2024. Benchmarking symbolic regression constant optimization schemes. *arXiv e-prints*, arXiv–2412.
- Gill, P. E.; and Murray, W. 1978. Algorithms for the solution of the nonlinear least-squares problem. *SIAM Journal on Numerical Analysis*, 15(5): 977–992.
- Golub, G. H.; and Pereyra, V. 2003. Separable nonlinear least squares: the variable projection method and its applications. *Inverse problems*, 19(2): R1.
- Grayeli, A.; Sehgal, A.; Reyes, O. C.; Cranmer, M.; and Chaudhuri, S. 2024. Symbolic Regression with a Learned Concept Library. In *The Thirty-eighth Annual Conference on Neural Information Processing Systems*.
- Guo, Z.; Wang, S.; Tian, Y.; Yang, J.; Yu, H.; Na, X.; Kovács, L.; Li, L.; Ioannou, P. A.; and Wang, F.-Y. 2025. SR-LLM: An incremental symbolic regression framework driven by LLM-based retrieval-augmented generation. *Proceedings of the National Academy of Sciences*, 122(52): e2516995122.
- Hayes, C. F.; Da Silva, F. L.; Yang, J.; Mundhenk, T. N.; Lee, C. S.; Pettit, J. F.; Santiago, C.; Kim, S.; Kim, J. T.; Solis, I. A.; et al. 2025. Deep Symbolic Optimization: Reinforcement Learning for Symbolic Mathematics. *arXiv preprint arXiv:2505.10762*.
- Hua, Y.; Li, R.; Yao, J.; Zhuang, G.; Tang, S.; Liu, B.; Ouyang, W.; and Lu, Y. 2025. Finetuning Large Language Model as an Effective Symbolic Regressor. arXiv:2508.09897.
- Huang, Z.; Huang, D. Z.; Xiao, T.; Ma, D.; Ming, Z.; Shi, H.; and Wen, Y. 2025. Improving Monte Carlo Tree Search for Symbolic Regression. In *The Thirty-ninth Annual Conference on Neural Information Processing Systems*.
- Ioannou, P.; Liò, P.; and Cicuta, P. 2026. An Empirical Investigation of Neural ODEs and Symbolic Regression for Dynamical Systems. arXiv:2601.20637.
- Kamienny, P.-A.; Lample, G.; Lamprier, S.; and Virgolin, M. 2023. Deep generative symbolic regression with monte-carlo-tree-search. In *International Conference on Machine Learning*, 15655–15668. PMLR.
- Kammerer, L.; Kronberger, G.; and Kommenda, M. 2022. Symbolic regression with fast function extraction and nonlinear least squares optimization. In *International Conference on Computer Aided Systems Theory*, 139–146. Springer.
- Kantor, D.; Von Zuben, F. J.; and de Franca, F. O. 2021. Simulated annealing for symbolic regression. In *proceedings of the genetic and evolutionary computation conference*, 592–599.
- Kommenda, M.; Burlacu, B.; Kronberger, G.; and Affenzeller, M. 2020. Parameter identification for symbolic regression using nonlinear least squares. *Genetic Programming and Evolvable Machines*, 21(3): 471–501.
- Koza, J. R. 1994. Genetic programming as a means for programming computers by natural selection. *Statistics and computing*, 4(2): 87–112.
- Kronberger, G.; and de Franca, F. O. 2025. Effects of reducing redundant parameters in parameter optimization for symbolic regression using genetic programming. *Journal of Symbolic Computation*, 129: 102413.
- Landajuela, M.; Lee, C.; Yang, J.; Glatt, R.; Santiago, C. P.; Aravena, I.; Mundhenk, T. N.; Mulcahy, G.; and Petersen, B. K. 2022. A Unified Framework for Deep Symbolic Regression. In *Advances in Neural Information Processing Systems*.
- Li, W.; Li, W.; Yu, L.; Wu, M.; Sun, L.; Liu, J.; Li, Y.; Wei, S.; Yusong, D.; and Hao, M. 2024. A Neural-Guided Dynamic Symbolic Network for Exploring Mathematical Expressions from Data. In Salakhutdinov, R.; Kolter, Z.; Heller, K.; Weller, A.; Oliver, N.; Scarlett, J.; and Berkenkamp, F., eds., *Proceedings of the 41st International Conference on Machine Learning*, volume 235 of *Proceedings of Machine Learning Research*, 28222–28242. PMLR.
- Loebl, J.; and Rozinajová, V. 2018. Continuous Cartesian Genetic Programming with Particle Swarm Optimization. In *International Conference on Intelligent Systems Design and Applications*, 985–995. Springer.
- Makke, N.; and Chawla, S. 2024. Interpretable scientific discovery with symbolic regression: a review. *Artificial Intelligence Review*, 57(1): 2.
- Martius, G.; and Lampert, C. H. 2016. Extrapolation and learning equations. *arXiv preprint arXiv:1610.02995*.

McConaghy, T. 2011. FFX: Fast, scalable, deterministic symbolic regression technology. In *Genetic Programming Theory and Practice IX*, 235–260. Springer.

Merler, M.; Haitsiukevich, K.; Dainese, N.; and Marttinen, P. 2024. In-Context Symbolic Regression: Leveraging Large Language Models for Function Discovery. In Fu, X.; and Fleisig, E., eds., *Proceedings of the 62nd Annual Meeting of the Association for Computational Linguistics (Volume 4: Student Research Workshop)*, 427–444. Bangkok, Thailand: Association for Computational Linguistics. ISBN 979-8-89176-097-4.

Petersen, B. K.; Landajuela, M.; Mundhenk, T. N.; Santiago, C. P.; Kim, S. K.; and Kim, J. T. 2021. Deep symbolic regression: Recovering mathematical expressions from data via risk-seeking policy gradients. In *Proc. of the International Conference on Learning Representations*.

Riley, A. B.; Webb, M.; and Baker, M. L. 2025. Deflation Techniques for Finding Multiple Local Minima of a Non-linear Least Squares Problem. *SIAM Journal on Scientific Computing*, 47(5): A2963–A2987.

Sahoo, S.; Lampert, C.; and Martius, G. 2018. Learning equations for extrapolation and control. In *International Conference on Machine Learning*, 4442–4450. Pmlr.

Schmidt, M.; and Lipson, H. 2009. Distilling free-form natural laws from experimental data. *science*, 324(5923): 81–85.

Sergeyev, Y. D.; Kvasov, D. E.; and Mukhametzhanov, M. S. 2016. On the least-squares fitting of data by sinusoids. In *Advances in stochastic and deterministic global optimization*, 209–226. Springer.

Sheta, A.; Abdel-Raouf, A.; Fraihat, K. M.; and Baareh, A. 2023. Evolutionary Design of a PSO-Tuned Multigene Symbolic Regression Genetic Programming Model for River Flow Forecasting. *Int. J. Adv. Comput. Sci. Appl*, 14: 806–814.

Shojaee, P.; Meidani, K.; Gupta, S.; Farimani, A. B.; and Reddy, C. K. 2025. LLM-SR: Scientific Equation Discovery via Programming with Large Language Models. In *The Thirteenth International Conference on Learning Representations*.

Stinstra, E.; Rennen, G.; and Teeuwen, G. 2008. Metamodeling by symbolic regression and Pareto simulated annealing. *Structural and Multidisciplinary Optimization*, 35(4): 315–326.

Udrescu, S.-M.; and Tegmark, M. 2020. AI Feynman: A physics-inspired method for symbolic regression. *Science advances*, 6(16): eaay2631.

Vaddireddy, H.; and San, O. 2019. Equation discovery using fast function extraction: a deterministic symbolic regression approach. *Fluids*, 4(2): 111.

Virgolin, M.; Alderliesten, T.; and Bosman, P. A. 2019. Linear scaling with and within semantic backpropagation-based genetic programming for symbolic regression. In *Proceedings of the genetic and evolutionary computation conference*, 1084–1092.

Zhang, H.; Chen, Q.; XUE, B.; Banzhaf, W.; and Zhang, M. 2025. RAG-SR: Retrieval-Augmented Generation for Neural Symbolic Regression. In *The Thirteenth International Conference on Learning Representations*.

## A SAGE-Fit Algorithm

The complete procedure of the SAGE-Fit evaluator described in Section 5.5 is presented in Algorithm 1. It integrates the three modules—structure-aware dimensionality reduction, semantics-guided initialization, and SR-specialized local attraction—into a unified pipeline that takes a candidate equation  $T$  together with data  $(\mathbf{X}, \mathbf{y})$  and returns a faithful score  $\hat{\mathcal{S}}(T)$  along with the fitted parameters  $(\hat{\alpha}, \hat{\beta})$ .

---

### Algorithm 1 SAGE-Fit Evaluator

---

**Require:** Candidate  $T$ , data  $(\mathbf{X}, \mathbf{y})$ , bounds  $[\ell, u]$ , oversampling parameter  $M = 100$ , number of starting points  $K = 8$

**Ensure:** Faithful score  $\hat{\mathcal{S}}(T)$  and parameters  $(\hat{\alpha}, \hat{\beta})$

- 1: **Module 1: Structure-Aware Dimensionality Reduction**
  - 2:  $(\alpha, \beta, \Phi, c) \leftarrow \text{ASTAFFINEPROPAGATION}(T)$  ▷ Eqs. (7)–(8)
  - 3: **Module 2: Semantics-Guided Initialization**
  - 4: Sample  $M$  candidates  $\{\beta_m\}_{m=1}^M$  around the warm-start initialization within  $[\ell, u]$
  - 5: **for**  $m = 1, \dots, M$  **do**
  - 6:    $\mathbf{f}_m \leftarrow f_T(\mathbf{X}; \alpha^*(\beta_m), \beta_m)$  ▷ Function-space evaluation
  - 7: **end for**
  - 8:  $\{\beta_{i_1}, \dots, \beta_{i_K}\} \leftarrow \text{FARTHESTPOINTSAMPLING}(\{\mathbf{f}_m\}, K)$  ▷ Eq. (11)
  - 9: **Module 3: SR-Specialized Local Attraction**
  - 10: **for**  $k = 1, \dots, K$  **in parallel do**
  - 11:    $\hat{\beta}_k \leftarrow \text{PROJECTEDTRF}(\beta_{i_k}, L_{\text{proj}})$  ▷ Eqs. (9),(10),(12)
  - 12: **end for**
  - 13:  $\hat{\beta} \leftarrow \arg \min_{\beta \in \{\hat{\beta}_1, \dots, \hat{\beta}_K\}} L_{\text{proj}}(\beta)$
  - 14:  $\hat{\alpha} \leftarrow \alpha^*(\hat{\beta})$  via Eq. (9)
  - 15:  $\hat{\mathcal{S}}(T) \leftarrow L_{\text{proj}}(\hat{\beta})$
  - 16: **return**  $(\hat{\mathcal{S}}(T), \hat{\alpha}, \hat{\beta})$
- 

## B LSR-Synth Dataset

The LSR-Synth dataset is designed to evaluate the true scientific equation discovery capability of large language model (LLM) based SR systems beyond memorization. Unlike benchmarks derived from well-known textbook equations, LSR-Synth introduces discovery-driven problems by combining established scientific terms with carefully constructed synthetic terms that are novel yet physically plausible.

**Scientific Domains** LSR-Synth spans four scientific domains: chemistry, biology, physics, and material science.

Chemistry problems focus on reaction kinetics and non-linear concentration–time dynamics. Biology tasks emphasize population dynamics and growth processes with non-linear regulatory effects. Physics equations are primarily drawn from dynamical systems, including oscillators, damping processes, and time-dependent forcing. Material science tasks cover stress–strain relationships, constitutive laws, and nonlinear material responses. Each domain is selected to reflect realistic scientific modeling scenarios while maintaining diversity in equation structure and operator usage. The final LSR-Synth dataset contains 128 problems across these four domains.

**Equation Construction Pipeline** The construction of LSR-Synth follows a multi-stage pipeline designed to ensure novelty, solvability, and scientific plausibility:

**(1) Scientific Problem Selection.** Representative scientific problems are first selected within each domain (e.g., reaction kinetics in chemistry or population growth in biology), along with a corresponding set of variables and physical interpretations.

**(2) Known Term Generation.** Given the problem description, a large language model is prompted to generate a set of commonly used and well-established mathematical terms that typically appear in standard formulations of the underlying scientific model.

**(3) Synthetic Term Generation.** In parallel, the LLM is prompted to generate synthetic terms that are novel in the given scientific context. These terms are designed to be mathematically valid and physically interpretable but are not part of standard textbook equations. Examples include higher-order nonlinearities, saturation effects, or unconventional time-dependent modulations.

**(4) Equation Assembly and Solvability Check.** Known terms and synthetic terms are combined into complete mathematical expressions. Each candidate equation is then verified for analytical or numerical solvability using numerical solvers (e.g., ODE solvers). Equations that are ill-posed or numerically unstable are discarded.

**(5) Novelty Verification.** To prevent trivial rediscovery or memorization, each constructed equation is evaluated for novelty using an LLM-based evaluator, which determines whether the equation requires data-driven reasoning rather than direct recall of known scientific laws.

**(6) Data Generation.** For equations that pass solvability and novelty checks, synthetic datasets are generated by numerically evaluating the equations under predefined parameter ranges and initial conditions. Both in-domain and out-of-domain (OOD) test sets are created when applicable to assess generalization.

**(7) Expert Validation.** Finally, the equations and their generated data are manually reviewed by subject matter experts to ensure scientific plausibility and consistency with the stated problem context.

**Symbolic Accuracy (SA)** Symbolic Accuracy (SA) is the primary metric used to evaluate whether a discovered equation is symbolically equivalent to the ground-truth equation in LSR-Synth. Unlike traditional SR recovery metrics that rely on exact string matching, SA focuses on semantic equivalence. Specifically, SA is computed using an LLM-based evaluator that compares the predicted equation and the ground-truth equation after removing numerical constants and fitted parameters. The evaluator determines whether the two expressions represent the same underlying mathematical relationship up to algebraic equivalence and parameterization. This evaluation protocol accounts for variations in expression form (e.g., reordering of terms or alternative but equivalent formulations) and is particularly well-suited for LLM-based equation discovery systems that may output equations in diverse symbolic representations. The reliability of SA is validated through comparison with human expert judgments, showing high agreement.